Phenomenological model of a 90° domain wall in $BaTiO_3$-type ferroelectrics

J. Hlinka and P. Márton
Institute of Physics, Academy of Sciences of the Czech Republic, Na Slovance 2, 18221 Praha 8, Czech Republic
(Received 26 May 2006; published 7 September 2006)

The properties of ferroelectric-ferroelastic twin boundaries in tetragonal $BaTiO_3$-like crystals are analyzed in the framework of the phenomenological Ginzburg-Landau-Devonshire model. Special attention is paid to the introduction and appreciation of the gradient and dipole-dipole terms, which depends on inhomogeneous polarization. An adjustment of the model parameters to the bulk properties of $BaTiO_3$ allows us to make quantitative predictions for domain-wall profiles and widths (at ambient conditions, 3.6 nm and 0.6 nm for fully relaxed 90° and 180° domain walls).

DOI: 10.1103/PhysRevB.74.104104 PACS number(s): 77.80.Dj, 77.84.Dy

I. INTRODUCTION

The 90° domain wall in tetragonal $BaTiO_3$ is a prototype example of a ferroelectric domain boundary separating two adjacent ferroelectric domains. In this well-known case, movement of the wall along its normal leads to rotation of both the direction of polarization and the orientation of the spontaneous strain tensor by about 90°. It has been recently demonstrated that these domain walls, if they are pinned[1,2] or sufficiently dense,[3–8] would lead to an extraordinary enhancement of the piezoelectric properties of $BaTiO_3$. Similar behavior is expected in other low-conductive ferroelectrics with ferroelectric-ferroelastic domain walls, and the same principle might be also behind the high-piezoelectric properties of relaxor-type materials with nanoscopic polar arrangement.

The preferred geometry of the 90° domain wall of $BaTiO_3$ is known to follow directly from basic energy considerations. To minimize the electrostatic energy in a insulating crystal, the polarization should have a head-to-tail arrangement so that there is no uncompensated charge at the wall (div $P=0$). Minimization of the elastic energy requires the 90° domain wall (which is also a ferroelastic twin boundary) to be planar and perpendicular to the sum of the polarization vectors of the adjacent domain states, in agreement with the general ferroelastic twin compatibility theory.[9,10] These rules are normally verified in experiments, although exceptions were reported in some special cases, too.[11–16]

More specific properties of the 90° domain wall of $BaTiO_3$ can be in principle addressed within the continuous Ginzburg-Landau-Devonshire-type model developed in a number of previous theoretical works.[17–25] While the continuous approach itself is well justified by the reasonably large thickness of the 90° domain wall in $BaTiO_3$ (according to available experimental and theoretical estimates,[17,26–33] in the range of 2–25 nm), its quantitative implications are largely dependent on the correct definition of the relevant terms in the model potential.

The aim of the present work is to assess the properties of the 90° domain wall of $BaTiO_3$ as much *quantitatively* as possible. For this purpose, we use the generalized Ginzburg-Landau-Devonshire-type model which includes long-range electrostatic interactions[34,35] (Sec. II), and utmost care is given to a realistic determination of all model parameters from the known bulk $BaTiO_3$ properties (Sec. III). Analytic and numerical solutions representing the equilibrium 90° domain wall are derived for the present model in Sec. IV. Section V is devoted to a discussion of the results and their detailed comparison with previous approaches and experiments.

II. PHENOMENOLOGICAL MODEL

We assume a proper ferroelectric crystal with a parent phase of macroscopically cubic O_h symmetry. The free energy of this system is assumed to be the sum of the part associated with a hypothetical reference cubic state F_r and the excess free energy F arising due to the nonzero primary and secondary order parameters (polarization and strain fields). Following several preceding works,[8,35,36,38,39] we complete the classical Landau-Ginzburg model for F by explicitly including the elastic, electrostrictive, and dipole-dipole terms. The resulting model for the excess free energy F is then given by a functional of Cartesian components of polarization P_i, its spatial derivatives $P_{i,j}=\partial P_i/\partial x_j$, and strain components $e_{ij}=(\partial u_i/\partial x_j+\partial u_j/\partial x_i)/2$, $i,j=1-3$, as follows:

$$F = F_{\mathrm{LG}}^{(e)}[\{P_i,P_{i,j}\}] + F_{\mathrm{Cq}}[\{P_i,e_{ij}\}] + F_{\mathrm{dep}}[\{P_i\}], \qquad (1)$$

where

$$F_{\mathrm{LG}}^{(e)}[\{P_i,P_{j,k}\}] = \int d\mathbf{r}[f_{\mathrm{L}}^{(e)}\{P_i\} + f_{\mathrm{G}}\{P_{i,j}\}] \qquad (2)$$

stands for the fully clamped Landau-Ginzburg potential,

$$F_{\mathrm{Cq}}[\{P_i,e_{ij}\}] = \int d\mathbf{r}[f_{\mathrm{C}}\{e_{ij}\} + f_{\mathrm{q}}\{P_i,e_{ij}\}] \qquad (3)$$

stands for the linear elastic and electrostriction energy, as considered, e.g., in the seminal paper of Devoshire,[39] and the nonlocal interaction term describing long-range electrostatic dipole-dipole interactions

$$F_{\mathrm{dep}}[\{P_i\}] = -\frac{1}{2}\int d\mathbf{r}[\mathbf{E}_{\mathrm{dep}}(\mathbf{r})\cdot\mathbf{P}(\mathbf{r})] \qquad (4)$$

depends on the inhomogeneous depolarization field $\mathbf{E}_{\mathrm{dep}}$, which can be expressed explicitly as a functional of $\mathbf{P}(\mathbf{r})$,

$$\mathbf{E}_{\mathrm{dep}}(\mathbf{r}) = -\frac{1}{4\pi\epsilon_0\epsilon_B}\int \mathbf{dr}'\left[\frac{\mathbf{P}(\mathbf{r}')}{|\mathbf{R}|^3} - \frac{\mathbf{3}(\mathbf{P}(\mathbf{r}')\cdot\mathbf{R})\mathbf{R}}{|\mathbf{R}|^5}\right], \quad (5)$$

with $\mathbf{R}=\mathbf{r}-\mathbf{r}'$.

This basic formulation assumes that there is no depolarization field associated with the overall polarization of the sample (as in the case of an infinite system or system with shortcut boundary conditions). In a more general situation, Eq. (5) for the depolarization field can be replaced by a solution of

$$\mathrm{div}\ \mathbf{E}_{\mathrm{dep}} = \frac{1}{\epsilon_B\epsilon_0}\ \mathrm{div}\ \mathbf{P} \quad (6)$$

under appropriate boundary conditions.

A. Devonshire free-energy density

The Landau-type free-energy density functional $f_{\mathrm{L}}^{(e)}$ is normally written as systematic-expansion O_h-symmetry-invariant terms in components of polarization P_i. In the case of $BaTiO_3$, discontinuity of the transition towards the paraelectric phase requires a model with terms up to at least sixth order:

$$\begin{aligned} f_{\mathrm{L}}^{(e)} &= \alpha_1(P_1^2+P_2^2+P_3^2) + \alpha_{11}^{(e)}(P_1^4+P_2^4+P_3^4) \\ &+ \alpha_{12}^{(e)}(P_1^2P_2^2+P_2^2P_3^2+P_1^2P_3^2) + \alpha_{111}(P_1^6+P_2^6+P_3^6) \\ &+ \alpha_{112}(P_1^4(P_2^2+P_3^2)+P_2^4(P_1^2+P_3^2)+P_3^4(P_1^2+P_2^2)) \\ &+ \alpha_{123}P_1^2P_2^2P_3^2. \end{aligned} \quad (7)$$

The coefficients of this expansion would generally depend on thermodynamic state variables such as temperature, external stress, or applied electric field, although often a linear temperature (or pressure) dependence of the α_1 coefficient is sufficient. Dependence on the strain order parameter is considered by including a bilinear elastic and electrostriction functionals[21,38,39] defined by elastic and electrostriction tensors C_{ijkl}, q_{ijkl}. It can be conveniently written in matrix notation[40] with Voigt abbreviated suffixes $\alpha=1-6$ ($e_1=e_{11}$, $e_2=e_{22}$, $e_3=e_{33}$, $e_4=2e_{23}$, $e_5=2e_{13}$, $e_6=2e_{12}$) as

$$\begin{aligned} f_{\mathrm{C}} &= \frac{1}{2}C_{ijkl}e_{ij}e_{kl} = \frac{1}{2}C_{\alpha\beta}e_\alpha e_\beta \\ &= \frac{1}{2}C_{11}[e_1^2+e_2^2+e_3^2] + C_{12}[e_2e_3+e_1e_3+e_1e_2] \\ &+ \frac{1}{2}C_{44}[e_4^2+e_5^2+e_6^2], \end{aligned} \quad (8)$$

$$\begin{aligned} f_{\mathrm{q}} &= -q_{ijkl}e_{ij}P_kP_l \\ &= -q_{11}[e_1P_1^2+e_2P_2^2+e_3P_3^2] \\ &- q_{12}[e_1(P_2^2+P_3^2)+e_2(P_1^2+P_3^2)+e_3(P_1^2+P_2^2)] \\ &- q_{44}[e_6P_1P_2+e_5P_1P_3+e_4P_2P_3], \end{aligned} \quad (9)$$

where $C_{11}=C_{1111}$, $C_{12}=C_{1122}$, $C_{44}=C_{1212}$, $q_{11}=q_{1111}$, $q_{12}=q_{1122}$, and $q_{44}=2q_{1212}$.

The equilibrium homogeneous state in applied homogeneous stress σ and electric field E is given by the minimum of the appropriate (incomplete) Gibbs free-energy density $g(T,\sigma,\mathbf{E};e,\mathbf{P})=f_{\mathrm{L}}^{(e)}+f_{\mathrm{C}}+f_{\mathrm{q}}-\sigma e-\mathbf{E}\cdot\mathbf{P}$—i.e., from the conditions

$$\frac{\partial}{\partial\mathbf{P}}(f_{\mathrm{L}}^{(e)}+f_{\mathrm{C}}+f_{\mathrm{q}}-\sigma\cdot e-\mathbf{E}\cdot\mathbf{P})=0,$$

$$\frac{\partial}{\partial e_\alpha}(f_{\mathrm{L}}^{(e)}+f_{\mathrm{C}}+f_{\mathrm{q}}-\sigma\cdot e-\mathbf{E}\cdot\mathbf{P})=0. \quad (10)$$

The second equation implies that the stress-free homogeneous equilibrium (spontaneous) strain at zero electric field is given by custom expressions

$$\begin{aligned} e_1 &= Q_{11}P_1^2+Q_{12}P_2^2+Q_{12}P_3^2, \\ e_2 &= Q_{12}P_1^2+Q_{11}P_2^2+Q_{12}P_3^2, \\ e_3 &= Q_{12}P_1^2+Q_{12}P_2^2+Q_{11}P_3^2, \\ e_4 &= Q_{44}P_2P_3, \\ e_5 &= Q_{44}P_3P_1, \\ e_6 &= Q_{44}P_1P_2, \end{aligned} \quad (11)$$

where the electrostriction coefficients Q_{ij} are expressed[39,41] through the bulk and shear elastic and electrostriction constants[21]

$$\begin{aligned} \hat{C}_{11} &= C_{11}+2C_{12}, \\ \hat{C}_{22} &= C_{11}-C_{12}, \\ \hat{q}_{11} &= q_{11}+2q_{12}, \\ \hat{q}_{22} &= q_{11}-q_{12}, \end{aligned} \quad (12)$$

as follows:[38]

$$\begin{aligned} Q_{11} &= Q_{1111} = 3^{-1}[\hat{q}_{11}/\hat{C}_{11}+2\hat{q}_{22}/\hat{C}_{22}], \\ Q_{12} &= Q_{1122} = 3^{-1}[\hat{q}_{11}/\hat{C}_{11}-\hat{q}_{22}/\hat{C}_{22}], \\ Q_{44} &= 4Q_{1212} = q_{44}/C_{44}. \end{aligned} \quad (13)$$

Substitution of Eq. (11) into Eqs. (8) and (9) gives two fourth-order invariant polynomials in polarization, so that the total free energy $f_{\mathrm{L}}=f_{\mathrm{L}}^{(e)}+f_{\mathrm{C}}+f_{\mathrm{q}}$ associated with stress-free homogeneous states has exactly the same form as $f_{\mathrm{L}}^{(e)}$ [Eq. (7)], apart from replacement of $\alpha_{11}^{(e)}$ and $\alpha_{12}^{(e)}$ coefficients by the renormalized ones:[38,39,42]

$$\begin{aligned} \alpha_{11} &= \alpha_{11}^{(e)} - \frac{1}{6}\left[\frac{\hat{q}_{11}^2}{\hat{C}_{11}}+\frac{2\hat{q}_{22}^2}{\hat{C}_{22}}\right], \\ \alpha_{12} &= \alpha_{12}^{(e)} - \frac{1}{6}\left[\frac{2\hat{q}_{11}^2}{\hat{C}_{11}}-\frac{2\hat{q}_{22}^2}{\hat{C}_{22}}+\frac{3q_{44}^2}{C_{44}}\right]. \end{aligned} \quad (14)$$

B. Nonlocal interactions

The Ginzburg functional $f_G(P_{i,j})$ contains the lowest-order symmetry-invariant terms in spatial derivatives of polarization, and it can be written in two frequently used equivalent forms

$$f_G = \frac{G_{11}}{2}(P_{1,1}^2 + P_{2,2}^2 + P_{3,3}^2) + G_{12}(P_{1,1}P_{2,2} + P_{2,2}P_{3,3} + P_{1,1}P_{3,3}) + \frac{G_{44}}{2}[(P_{1,2} + P_{2,1})^2 + (P_{2,3} + P_{3,2})^2 + (P_{3,1} + P_{1,3})^2] \quad (15)$$

or, with a new[38] constant $G_{14}=G_{12}+G_{44}$, as

$$f_G = \frac{G_{11}}{2}(P_{1,1}^2 + P_{2,2}^2 + P_{3,3}^2) + G_{14}(P_{1,1}P_{2,2} + P_{2,2}P_{3,3} + P_{1,1}P_{3,3}) + \frac{G_{44}}{2}[P_{1,2}^2 + P_{2,1}^2 + P_{2,3}^2 + P_{3,2}^2 + P_{3,1}^2 + P_{1,3}^2]. \quad (16)$$

The former expression is a formal analog of the elastic energy density [Eq. (8)]; the latter expression has a more straightforward interpretation in its discrete form. Assuming a discrete polarization field on a simple cubic lattice, the spatial derivatives are replaced by first-neighbor finite differences. In the lowest-order approximation, one can retain only the two first-neighbor symmetry-allowed pairwise harmonic terms—longitudinal and transverse coupling terms, which correspond to the G_{11} and G_{44} terms in the latter expression, respectively. The fact that the G_{14} cross term drops out in this basic and natural approximation suggests that it is not a very important term, but it can be obviously easily included if necessary—e.g., in second-neighbor approximations. Let us finally mention that some authors[34,38,43] are including in the expression (15) also the G'_{44} term

$$\frac{1}{2}G'_{44}[(P_{1,2} - P_{2,1})^2 + (P_{2,3} - P_{3,2})^2 + (P_{3,1} - P_{1,3})^2]. \quad (17)$$

However, this term can be actually transformed into a combination of G_{12} and G_{44} terms (its action is equivalent to the replacements $G_{44} \rightarrow G_{44}+G'_{44}$, $G_{12} \rightarrow G_{12}-2G'_{44}$), because the volume integral of the $P_{1,2}P_{2,1}$ term is equal to that of the $P_{1,1}P_{2,2}$ one. This means that only the symmetrical part of the $P_{i,j}$ matrix contributes to the gradient energy, and, therefore, the Ginzburg functional can be written as

$$f_G = \frac{1}{2}G_{ijkl}P_{i,j}P_{k,l}, \quad (18)$$

where G_{ijkl} is same type of fourth-rank symmetric tensor as C_{ijkl} (and where $G_{11}=G_{1111}$, $G_{12}=G_{1122}$, and $G_{44}=G_{1212}$, but G_{14}, as introduced[38] before, is not equal to G_{1123}).

TABLE I. Complete list of parameters describing the phenomenological model defined by Eqs. (1)–(9). Three sets of numerical values (cited as models I, II, and III) for room-temperature $BaTiO_3$ are derived in the text.

	I	II	III	Unit [SI]
α_1	−2.772	−2.772	−3.712	10^7 J m C^{-2}
α_{11}	−6.476	−6.476	−2.097	10^8 J m^5 C^{-4}
$\alpha_{11}^{(e)}$	1.701	2.199	6.079	10^8 J m^5 C^{-4}
α_{12}	3.23	3.23	7.974	10^8 J m^5 C^{-4}
$\alpha_{12}^{(e)}$	−3.441	−4.360	1.303	10^8 J m^5 C^{-4}
α_{111}	8.004	8.004	1.294	10^9 J m^9 C^{-6}
α_{112}	4.47	4.47	−1.950	10^9 J m^9 C^{-6}
α_{123}	4.91	4.91	−2.500	10^9 J m^9 C^{-6}
α_{1111}			3.863	10^{10} J m^{13} C^{-8}
α_{1112}			2.529	10^{10} J m^{13} C^{-8}
α_{1122}			1.637	10^{10} J m^{13} C^{-8}
α_{1123}			1.367	10^{10} J m^{13} C^{-8}
G_{11}	51	51	51	10^{-11} J m^3 C^{-2}
G_{12}	−2	−2	−2	10^{-11} J m^3 C^{-2}
G_{44}	2	2	2	10^{-11} J m^3 C^{-2}
q_{11}	14.20	13.62	14.20	10^9 J m C^{-2}
q_{12}	−0.74	−2.56	−0.74	10^9 J m C^{-2}
q_{44}	1.57	1.62	1.57	10^9 J m C^{-2}
C_{11}	27.50	21.10	27.50	10^{10} J m^{-3}
C_{12}	17.90	10.70	17.90	10^{10} J m^{-3}
C_{44}	5.43	5.60	5.43	10^{10} J m^{-3}
ϵ_B	7.35	7.35	7.35	

III. MODEL PARAMETERS FOR $BaTiO_3$

The parameters in the above model can be estimated from bulk single-crystal properties. The ambient condition values for $BaTiO_3$ crystal, which are used in this paper, are resumed in Table I.

For the parameters of the the Landau functional, we have adopted set of values used in Refs. 42 and 44 (sixth-order expansion, models I and II in Table I) or that of in Ref. 45 (eighth-order expansion, model III in Table I), assuming $T=298$ K and taking into account the renormalizations given by Eqs. (14). These Landau potentials are considered quite realistic as they qualitatively reproduce the actual (temperature–electric-field) phase diagram as well as $E=0$ transition entropies,[45] although they may obviously fail to describe some higher-order effects.[75]

The values of elastic and electrostriction tensors C_{ij}, q_{ij} in models I and III are taken as in Ref. 35. These elastic constants are thus in fact[46] room-temperature $C_{ij}^{\mathbf{E}}$ values of Ref. 47. In model II, we have adopted the $C_{ij}^{\mathbf{E}}$ values of a more recent Brillouin experiment.[46] Other recent measurements[48,49] also give similar values. All these values are obviously somewhat renormalized by the electrostriction, but we are not aware of complete measurements of the tem-

perature dependence of C_{ij} and q_{ij} tensors in the cubic phase of $BaTiO_3$, which in principle would allow one to take proper renormalization into account. In any case, the most relevant are the resulting values of the electrostriction coefficients $Q_{\alpha\beta}$. In all three parameter sets, the selected parameters of C_{ij} and q_{ij} give electrostriction coefficients $Q_{\alpha\beta}$ identical to those considered in Ref. 41 (actually, derived[50] from results of Ref. 47) and very close to the electrostriction coefficients used in the recent Ref. 45.

The choice of coefficients G_{11}, G_{12}, and G_{44} of the gradient terms and the relative permittivity ϵ_B in the expression for the dipole-dipole interaction deserves some more caution. In order to adjust the parameter values of the gradient terms, one can use the soft phonon dispersion measured by inelastic neutron scattering as was proposed, for instance, in Refs. 24 and 51. In the soft-mode theory, small fluctuations of the order parameter are identified with soft-phonon modes. For example, in the case of the potential considered here, dispersion of transverse soft-phonon modes with wave vectors $\mathbf{q}$ parallel to the [100] and [111] directions, respectively, are in the paraelectric phase given by[51]

$$\zeta\omega_{[100]}^2 = 2\alpha_1 + G_{44}q^2, \tag{19}$$

$$\zeta\omega_{[111]}^2 = 2\alpha_1 + \frac{1}{3}(G_{11} - G_{12} + 2G_{44})q^2, \tag{20}$$

where $\zeta^{-1}=\epsilon_0\Omega_p^2$ is a common factor including mode-effective charge and mass via the mode-plasma frequency Ω_p as defined, e.g., in Ref. 52. On the other hand, the corresponding phonon dispersion curves as obtained in the inelastic neutron study[53] of cubic $BaTiO_3$ can be approximated as (at 150 °C)

$$(\hbar\omega_{[100]})^2 = (3\ \text{meV})^2 + 970\ (\text{meV Å})^2 q^2, \tag{21}$$

$$(\hbar\omega_{[111]})^2 = (3\ \text{meV})^2 + 5500\ (\text{meV Å})^2 q^2. \tag{22}$$

Using the $\alpha_1(150\ °\text{C}) \approx 1.4\times10^7$ value according to the Ref. 41, comparison of Eqs. (19) and (21) allows us to evaluate independently $\hbar\Omega_p \approx 190$ meV and $G_{44} \approx 3\times10^{-11}$ m^4 N C^{-2}. The value of the mode-plasma frequency is quite close to the values evaluated for the $BaTiO_3$ soft mode from room-temperature IR reflectivity data[52] ($\hbar\Omega_p \approx 200$ meV) as well as to the mode-plasma frequency of the pure Slater mode calculated[52] directly from *ab initio*–predicted Born effective charges[54] ($\hbar\Omega_p \approx 190$ meV). Therefore, the estimation of G_{44} appears also quite reliable. In addition, an alternative estimation ($G_{44}=2\alpha_1\xi_{44} \approx 3.5\times10^{-11}$ m^4 N C^{-2}) can be obtained using correlation length ξ_{44} from a neutron diffuse scattering experiment[55] (at 137 °C, $\alpha_1=9.7\times10^6$, $\xi_{44}\approx 13.5$ Å). It should be stressed that the $\omega_{[100]}^2$ branch is significantly mixed with a transverse acoustic branch. This mixing is disentangled in Ref. 53 so that the parameters shown above describe the dispersion of the bare optic branch. It is known[56,57] that after the elimination of the strain field from the Landau-Ginzburg potential, the TA-TO interaction effectively decreases the values of the gradient terms in polarization, and since the TA-TO interaction is not considered explicitly in the present model potential, one should use an effective G_{44} value. Following the calculations of Ref. 57 and using the coupling parameters of Table 1 in Ref. 53, we estimate that this flexoelectric reduction of G_{44} is in $BaTiO_3$ of the order of 25%–30%. This is much less than in the case[57] of $SrTiO_3$, but in order to take this effect into account we use a slightly lower value of $G_{44}=2\times10^{-11}$ m^4 N C^{-2}.

The dispersion parameter of $\omega_{[111]}^2$ (22) was read out directly from Fig. 8 in Ref. 53. It allows one to estimate $G_{11}-G_{12}+2G_{44}\approx 51\times10^{-11}$ m^4 N C^{-2}. Assuming that the first-neighbor interactions are essential ($G_{14}=0$, $G_{12}=-G_{44}$), we finally have $G_{11}\approx 45\times10^{-11}$ m^4 N C^{-2}. The pronounced difference between G_{11} and G_{44} values is associated with the huge anisotropy of the soft-mode dispersion curves and it reveals a large dipole-dipole contribution related to the large mode-effective charge of the soft mode, typical for $BaTiO_3$-type perovskites. Similar numerical values of G_{ii} can be deduced also from the *ab initio*–calculated zero-temperature imaginary dispersion curves of the soft-mode branches in the unstable cubic state, such as, e.g., from data of Ref. 54.

The expression of electrostatic dipole-dipole energy density has a single adjustable parameter—the "background" dielectric permittivity ϵ_B. It allows us to include all the additional high-frequency susceptibility contributions which are not associated with the soft mode—the electronic permittivity and eventually also the permittivity due to other high-frequency polar lattice modes. In the ferroelectric phase, ϵ_B should actually be considered as a tensor. According to the room-temperature IR reflectivity data[58] of $BaTiO_3$, the values of ϵ_B are 7.71 and 6.62 for an electric field oriented perpendicular and parallel to the polarization, respectively. In this paper, we neglect the anisotropy and the isotropic average of these values is taken for ϵ_B. The dipole-dipole contribution obviously leads to the LO-TO splitting of the soft-mode optic branch, and its magnitude in the present model $(\hbar\Omega_{LO})^2-(\hbar\Omega_{TO})^2=(\hbar\Omega_P)^2/\epsilon_B=(70\ \text{meV})^2$ is then slightly lower than that of the bare E_{TO} mode evaluated with average electronic contribution [about $(79\ \text{meV})^2$]. Let us stress that some authors considered $\epsilon_B=1$ but taking ϵ_B equal to static susceptibility as proposed in Refs. 34, 59, and 60 is not satisfactory at all since the dipole-dipole interactions would lead to an unrealistic LO-TO splitting of the soft-phonon branch of an insulating system.

IV. DOMAIN-WALL PROFILES

The above-described model allows us to calculate the phase diagram and basic single-domain properties. In the model with sixth-order Landau potential expansion, the number of quantities can be in fact obtained as very simple explicit expressions. For example, the spontaneous polarization of a fully relaxed (stress-free) single-domain and short-circuited state is given by

$$P_0^2 = \frac{-\alpha_{11} + \sqrt{(\alpha_{11})^2 - 3\alpha_1\alpha_{111}}}{3\alpha_{111}}, \tag{23}$$

the associated components of tetragonal spontaneous strain (along and perpendicular to the spontaneous polarization) are given by

TABLE II. Several quantities derived for different sets of model parameters given in Table I.

	I	II	III	Unit
P_0	0.265	0.265	0.260	C m^{-2}
$e_{\parallel}$	7.78	7.78	7.45	10^{-3}
$e_{\perp}$	−3.18	−3.18	−3.05	10^{-3}
$\hat{q}_{11}$	1.272	0.850	1.272	10^{10} J m C^{-2}
$\hat{q}_{22}$	1.494	1.818	1.494	10^{10} J m C^{-2}
$\hat{C}_{11}$	63.30	42.50	63.30	10^{10} J m^{-3}
$\hat{C}_{22}$	9.60	10.04	9.60	10^{10} J m^{-3}
Q_{11}	11.04	11.04	11.04	10^{-2} m^4 C^{-2}
Q_{12}	−4.52	−4.52	−4.52	10^{-2} m^4 C^{-2}
Q_{44}	2.89	2.89	2.89	10^{-2} m^4 C^{-2}

$$e_{\parallel} = Q_{11}P_0^2, \quad e_{\perp} = Q_{12}P_0^2, \tag{24}$$

and the associated excess Gibbs free-energy density reads

$$f_{\mathrm{T\ min}} = -P_0^4(\alpha_{11} + 2\alpha_{111}P_0^2). \tag{25}$$

The numerical values of these quantities are for room-temperature $BaTiO_3$ given in Table II. A similar analysis can be obviously performed numerically or analytically for other plausible phases as a function of temperature, pressure,[61] chemical substitution,[62] or more general mechanical conditions (such as, for example, biaxial clamping by substrate in case of thin films[63]).

Our interest here is rather in the variational problem $\delta F = 0$ and its kink-type solutions corresponding to domain walls separating adjacent tetragonal domain states. Such solutions have to obey Euler-Lagrange equations, ensuring local mechanical equilibrium conditions for polarization and strain. In the absence of the dipole-dipole interaction term F_{dep}, these equations have the standard form

$$\frac{\partial}{\partial x_j}\left(\frac{\partial f}{\partial P_{i,j}}\right) = \frac{\partial f}{\partial P_i}, \tag{26}$$

$$\frac{\partial}{\partial x_j}\left(\frac{\partial f}{\partial e_{ij}}\right) = 0, \tag{27}$$

with $f = f_{\mathrm{L}}^{(e)} + f_{\mathrm{G}} + f_{\mathrm{C}} + f_{\mathrm{q}}$. We will focus on the 90° domain wall and thus closely follow and develop the approach presented earlier in papers by Zhirnov,[17] Ishibashi,[19] Cao and Cross,[21] and Ishibashi and Salje.[18] We shall consider a (110)-domain wall (normal to the $x+y$ direction), corresponding to rotation of the spontaneous polarization by about 90° around the z axis, as sketched in Fig. 1 (90° head-to-tail ferroelastic domain wall). In other words, we are seeking a quasi-one-dimensional, single-kink-type solution described by the polarization field $[P_1(x+y), P_2(x+y), 0]$ such that, for $x+y \to -\infty$,

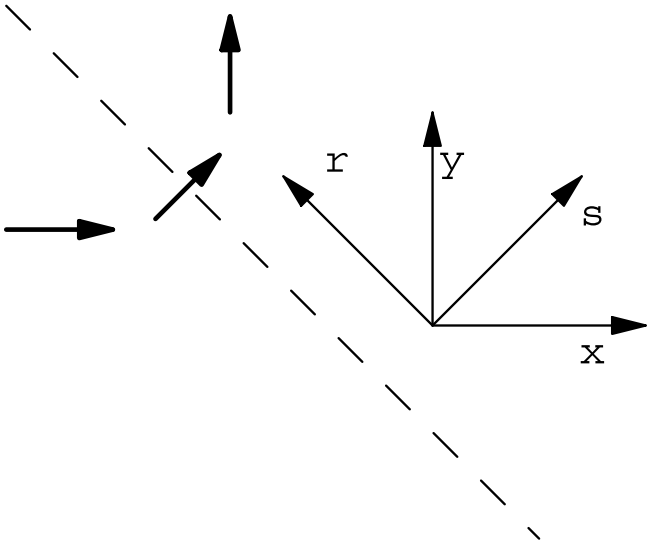

FIG. 1. (001) cross section through a head-to tail, (110)- oriented 90° twin boundary in $BaTiO_3$-type crystal. Polarizations in domains and in the boundary are shown schematically by thick arrows; the dashed line stands for the center of the wall. Thin arrows indicate the orientation of new and old axes.

$$[P_1, P_2, 0] \to [P_0, 0, 0],$$

$$[e_1, e_3, e_3, e_4, e_5, e_6] \to [e_{\parallel}, e_{\perp}, e_{\perp}, 0, 0, 0] \tag{28}$$

and, for $x+y \to +\infty$,

$$[P_1, P_2, 0] \to [0, P_0, 0],$$

$$[e_1, e_3, e_3, e_4, e_5, e_6] \to [e_{\perp}, e_{\parallel}, e_{\perp}, 0, 0, 0]. \tag{29}$$

The problem is conveniently solved in a 45°-rotated Cartesian-coordinate system s-r-z, where (see Fig. 1)

$$x' = s = (x + y)/\sqrt{2},$$

$$y' = r = (y - x)/\sqrt{2},$$

$$P_{1'} = P_s = (P_1 + P_2)/\sqrt{2},$$

$$P_2' = P_r = (P_2 - P_1)/\sqrt{2}. \tag{30}$$

In the rotated system, components of the elastic tensor are given by

$$C'_{\alpha\beta} = \begin{pmatrix} C'_{11} & C'_{12} & C_{12} & 0 & 0 & 0 \\ C'_{12} & C'_{11} & C_{12} & 0 & 0 & 0 \\ C_{12} & C_{12} & C_{11} & 0 & 0 & 0 \\ 0 & 0 & 0 & C_{44} & 0 & 0 \\ 0 & 0 & 0 & 0 & C_{44} & 0 \\ 0 & 0 & 0 & 0 & 0 & C'_{66} \end{pmatrix}, \tag{31}$$

with

$$C'_{11} = \frac{C_{11} + C_{12} + 2C_{44}}{2},$$

$$C'_{12} = \frac{C_{11} + C_{12} - 2C_{44}}{2},$$

$$C'_{66} = \frac{C_{11} - C_{12}}{2}, \tag{32}$$

and the elastic energy can be expressed as

$$f_C = \frac{1}{2} C'_{\alpha\beta} e'_\alpha e'_\beta, \tag{33}$$

where e'_α are strain tensor components in the rotated Cartesian system. Voigt matrices of electrostriction and gradient tensors have the same structure as that of an elastic tensor [Eq. (31)], with

$$q'_{11} = \frac{q_{11} + q_{12} + q_{44}}{2},$$

$$q'_{12} = \frac{q_{11} + q_{12} - q_{44}}{2},$$

$$q'_{66} = q_{11} - q_{12},$$

$$G'_{11} = \frac{G_{11} + G_{12} + 2G_{44}}{2},$$

$$G'_{12} = \frac{G_{11} + G_{12} - 2G_{44}}{2},$$

$$G'_{66} = \frac{G_{11} - G_{12}}{2}. \tag{34}$$

Boundary conditions and Saint-Venant compatibility relations restrict the single-kink, quasi-one-dimensional solution of the Euler-Lagrange equation for strain components [Eq. (27)] e'_α in the form[17,21] where only e'_1 and e'_6 follow the inhomogeneous polarization profiles $P_r(s)$ and $P_s(s)$,

$$e'_1 = \frac{e_\perp + e_\parallel}{2} - \frac{q_{11} + q_{12}}{2C'_{11}}(P_0^2 - P_r^2 - P_s^2) + \frac{q_{44}}{2C'_{11}}(P_s^2 - P_r^2),$$

$$e'_6 = \frac{2\hat{q}_{22}}{\hat{C}_{22}} P_r P_s, \tag{35}$$

while the remaining components do not change across the domain wall and they are just equal to the above-defined boundary values:

$$e'_2 = \frac{1}{2}(e_\perp + e_\parallel),$$

$$e'_3 = e_\perp,$$

$$e'_4 = e'_5 = 0. \tag{36}$$

This formal solution can be inserted to the Euler-Lagrange equations (26) for the polarization. It results in a pair of coupled differential equations[17,21] for $P_r(s)$ and $P_s(s)$. For the model with a sixth-order Landau expansion, these equations were derived in Ref. 21:

$$G'_{11} P_{s,ss} = 2\alpha_1^s P_s + 4\alpha_{11}^s P_s^3 + 2\alpha_{12}^{sr} P_s P_r^2 + 6\alpha'_{111} P_s^5 + 4\alpha'_{112} P_s^3 P_r^2 + 2\alpha'_{112} P_s P_r^4,$$

$$G'_{66} P_{r,ss} = 2\alpha_1^r P_r + 4\alpha_{11}^r P_r^3 + 2\alpha_{12}^{sr} P_r P_s^2 + 6\alpha'_{111} P_r^5 + 4\alpha'_{112} P_r^3 P_s^2 + 2\alpha'_{112} P_r P_s^4, \tag{37}$$

with coefficients

$$\alpha_1^s = \alpha_1 - \left[\frac{1}{3}\frac{\hat{q}_{11}^2}{\hat{C}_{11}} + \frac{1}{6}\frac{\hat{q}_{22}^2}{\hat{C}_{22}} - \frac{(q_{11} + q_{12})q'_{11}}{2C'_{11}}\right] P_0^2,$$

$$\alpha_1^r = \alpha_1 - \left[\frac{1}{3}\frac{\hat{q}_{11}^2}{\hat{C}_{11}} + \frac{1}{6}\frac{\hat{q}_{22}^2}{\hat{C}_{22}} - \frac{(q_{11} + q_{12})q'_{12}}{2C'_{11}}\right] P_0^2,$$

$$\alpha_{11}^s = \frac{\alpha_{11}^{(e)}}{2} + \frac{\alpha_{12}^{(e)}}{4} - \frac{q'^2_{11}}{2C'_{11}},$$

$$\alpha_{11}^r = \frac{\alpha_{11}^{(e)}}{2} + \frac{\alpha_{12}^{(e)}}{4} - \frac{q'^2_{12}}{2C'_{11}},$$

$$\alpha_{12}^{sr} = 3\alpha_{11}^{(e)} - \frac{\alpha_{12}^{(e)}}{2} - \frac{q'_{11}q'_{12}}{C'_{11}} - \frac{\hat{q}_{22}^2}{\hat{C}_{22}},$$

$$\alpha'_{111} = \frac{\alpha_{111} + \alpha_{112}}{4},$$

$$\alpha'_{112} = (15\alpha_{111} - \alpha_{112})/4. \tag{38}$$

Analytical solutions of Eqs. (37) were found in special cases only. For example, Ref. 21 considers the case when the α_{12}^{sr} and α'_{112} coefficients are simultaneously equal to zero, while Ref. 17 assumes $P_s \equiv P_0/\sqrt{2}$. Both assumptions lead to decoupling and to the same type of solution

$$P_s = \frac{1}{\sqrt{2}} P_0, \tag{39}$$

$$P_r = \frac{1}{\sqrt{2}} P_0 \frac{\sinh(s/\xi')}{[A + \sinh^2(s/\xi')]^{-1/2}}. \tag{40}$$

In a general case, exact solutions can be found numerically. For example, in Fig. 2 we give numerical solutions for the $BaTiO_3$ potential parameters (model I, without dipole-dipole interactions).

Several general properties are apparent from the first integral of the Euler-Lagrange equations, which can be written as follows:

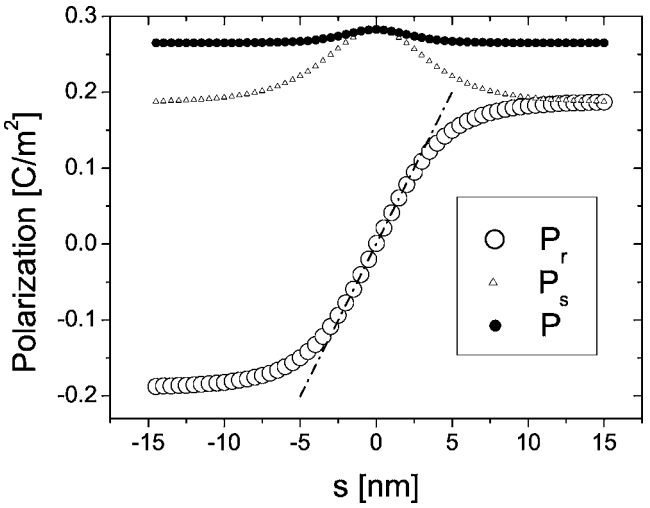

FIG. 2. Polarization profiles across a 90° head-to-tail domain wall in room-temperature $BaTiO_3$ calculated *without* long-range dipole-dipole interactions (using parameter set I of Table I). Larger point symbols stay for P_r, smaller ones for P_s and $P=|\mathbf{P}|=\sqrt{P_s^2+P_r^2}$, respectively. The dash-dotted line indicates the meaning of the domain-wall thickness defined in Eq. (43).

$$\frac{G'_{11}}{2}P_{s,s}^2+\frac{G'_{66}}{2}P_{r,s}^2=f_{EL}[P_s,P_r]-f_{EL0}. \tag{41}$$

Here the "Euler-Lagrange potential" $f_{EL}[P_s,P_r]$ and the integration constant f_{EL0}, determined from boundary conditions [Eqs. (28) and (29)], reads

$$f_{EL}[P_s,P_r]=\alpha_1^s P_s^2+\alpha_1^r P_r^2+\alpha_{11}^s P_s^4+\alpha_{11}^r P_r^4+\alpha_{12}^{sr}P_s^2P_r^2 + \alpha'_{111}(P_s^6+P_r^6)+\alpha'_{112}P_s^2P_r^2(P_s^2+P_r^2),$$

$$f_{EL0}=f_{EL}[P_0/\sqrt{2},P_0/\sqrt{2}]. \tag{42}$$

The shape of the Euler-Lagrange potential $f_{EL}[P_s,P_r]$ for $BaTiO_3$ parameters is apparent from the Fig. 3. By definition, it has two minima I and II, corresponding to the domain states selected as boundary conditions [Eqs. (28) and (29), respectively]. The searched for solution of the Euler-Lagrange equation can be considered as a least-action path connecting these domain states. As the f_{EL} potential is symmetric with respect to the $P_r=0$ plane, it is natural to define the $P_r=0$ point of the trajectory as the center of the domain wall. Let us associate this state with $s=0$. Then, the P_r component of the solution is an odd function of s. Since the exact shape of $P_r(s)$ not known, it is convenient to define[76] the domain-wall thickness via the derivative of the switched polarization component at the domain-wall center:

$$2\xi_{HT}=2\left[\frac{1}{P_{r\infty}}\left(\frac{\partial P_r}{\partial s}\right)_{s=0}\right]^{-1}, \tag{43}$$

where $P_{r\infty}=\lim_{s\to\infty}P_r(s)=P_0/\sqrt{2}$. The motivation for this definition is apparent from Fig. 2. In the special case of Eq. (40), it gives just $2\xi_{HT}=2\xi'\sqrt{A}$.

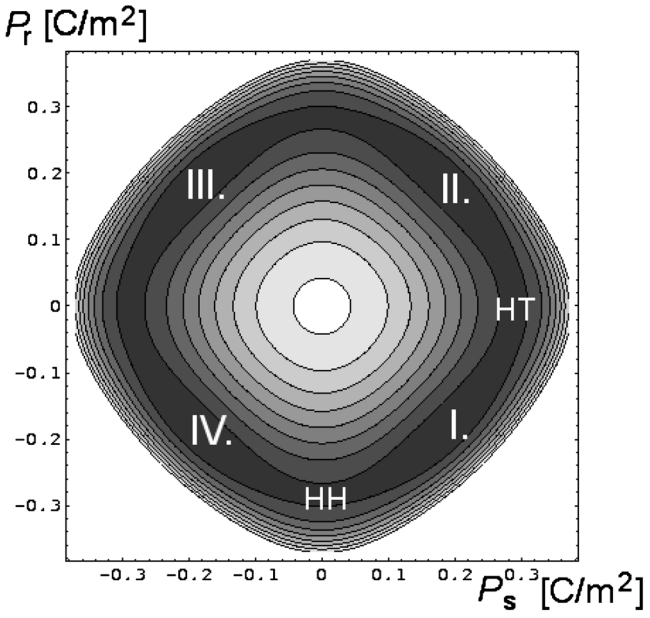

FIG. 3. Euler-Lagrange potential $f_{EL}[P_s,P_r]$ for model I but *without* long-range dipole-dipole interactions. Minima I and II correspond to domain states selected as boundary conditions. The state denoted HT (HH) corresponds to the polarization state in the center of the head-to-tail (head-to head) domain wall.

The same Euler-Lagrange potential appears in the calculation of other types of (110)-oriented 90° domain walls. For example, replacement of Eq. (29) by a new $x+y\to+\infty$ boundary condition

$$[P_1,P_2,0]\to[0,-P_0,0],$$

$$[e_1,e_3,e_3,e_4,e_5,e_6]\to[e_\perp,e_\parallel,e_\perp,0,0,0] \tag{44}$$

defines the head-to-head domain-wall solution, which corresponds to the I↔IV trajectory, passing through a "head-to-head" domain-wall center HH (see Fig. 3).

The magnitude of polarization in the center of the head-to-head (head-to-tail) domain wall is given by

$$P_{HT1}^2=\frac{-\alpha_{11}^s+\sqrt{(\alpha_{11}^s)^2-3\alpha_1^s\alpha'_{111}}}{3\alpha'_{111}},$$

$$P_{HH1}^2=\frac{-\alpha_{11}^r+\sqrt{(\alpha_{11}^r)^2-3\alpha_1^r\alpha'_{111}}}{3\alpha'_{111}}, \tag{45}$$

and the associated f_{EL} values are

$$f_{HT1}=-P_{HT1}^4(\alpha_{11}^r+2\alpha'_{111}P_{HT1}^2),$$

$$f_{HH1}=-P_{HH1}^4(\alpha_{11}^s+2\alpha'_{111}P_{HH1}^2). \tag{46}$$

Using the first integral of the Euler-Lagrange equations, the domain-wall thicknesses can be expressed as

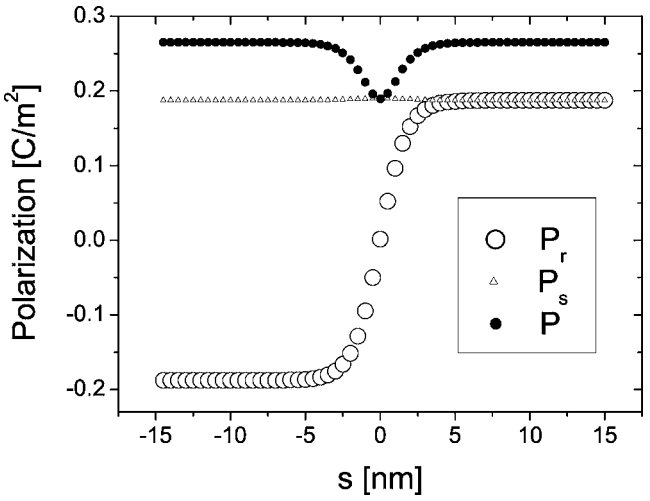

FIG. 4. Polarization profiles across a 90° head-to-tail domain wall in room-temperature $BaTiO_3$ calculated for the present model *including* the dipole-dipole term using parameter set I of Table I. Larger point symbols stay for P_r, smaller ones for P_s and $|\mathbf{P}|$, respectively.

$$2\xi_{HT1} = P_0\sqrt{\frac{G'_{66}}{f_{HT1} - f_{EL0}}},$$

$$2\xi_{HH1} = P_0\sqrt{\frac{G'_{11}}{f_{HH1} - f_{EL0}}}. \tag{47}$$

Let us stress that although the head-to-head and head-to-tail domain walls are found equivalent in some simplified models, in general they have distinct energies and thicknesses already at the level of the Landau-Ginzburg-Devonshire model. The difference between thicknesses can arise either because a general anisotropy of the gradient tensor ($G'_{66}=G'_{11}$ only if $G_{44}+G_{12}=0$) or because of a general anisotropy of electrostriction tensor ($q_{44}\neq 0$). In the case of $BaTiO_3$, however, these differences are negligible, and the real effect is due to the inhomogeneous depolarization field F_{dep} associated with charge on head-to-head domain walls (compare Fig. 2 and Fig. 4). Such a depolarization field can be evaluated from Eq. (6) with appropriate boundary conditions. Assuming as, e.g., in Ref. 18 that the depolarization field is zero (compensated) in the domain state I, the resulting Euler-Lagrange potential including the depolarization energy contribution reads

$$f_{EL2} = f_{EL} + \frac{1}{2\epsilon_B\epsilon_0}(P_s - P_0/\sqrt{2})^2. \tag{48}$$

This contribution can drastically change the shape of the Euler-Lagrange potential. In our room-temperature $BaTiO_3$ model, the minima II and IV are in fact completely eliminated (see Fig. 5) so that only head-to-tail (and tail-to-head) domain walls are permissible. Simultaneously, the saddle-point polarization is pushed towards to $P_0/\sqrt{2}$ and the charge-neutral condition of Zhirnov ($P_s \equiv P_0/\sqrt{2}$) thus becomes quite a good approximation. Within this approximation, the Euler-lagrange equation for P_r (in model sixth-order Landau expansion) reads

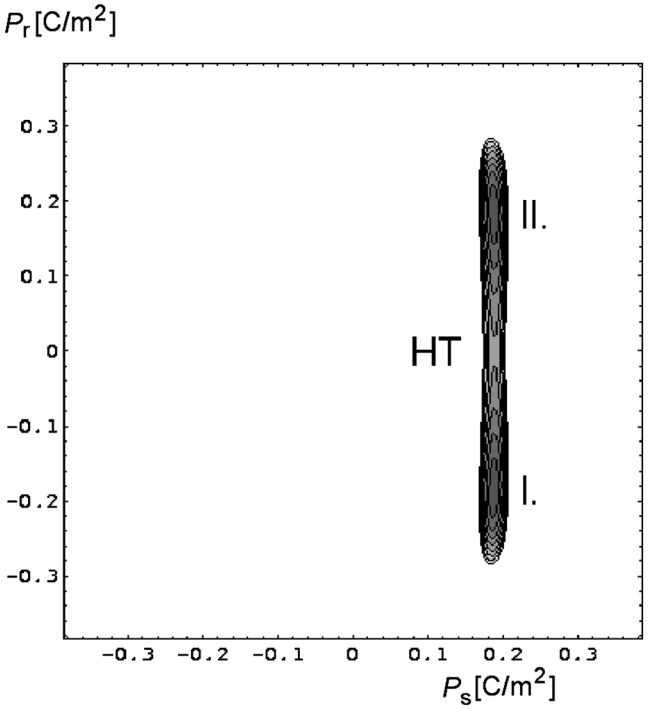

FIG. 5. Euler-Lagrange potential $f_{EL2}[P_s, P_r]$ for model I but *including* long-range dipole-dipole interactions. Minima I and II correspond to domain states selected as boundary conditions.

$$G'_{66}P_{r,ss} = 2\alpha_1^{cn}P_r + 4\alpha_{11}^{cn}P_r^3 + 6\alpha'_{111}P_r^5, \tag{49}$$

where

$$\alpha_1^{cn} = \alpha_1^r + \alpha_{12}^{sr}P_0^2 + 0.25\alpha'_{112}P_0^4,$$

$$\alpha_{11}^{cn} = \alpha_{11}^r + \alpha_{12}^{sr}P_0^2 + 0.5\alpha'_{112}P_0^2, \tag{50}$$

and it has thus the simple solution [Eq. (40)] with

$$\xi' = \frac{1}{P_0}\sqrt{\frac{G'_{66}}{6\alpha'_{111}P_0^2 + \alpha_{11}^{cn}}},$$

$$A = \frac{6\alpha'_{111}P_0^2 + \alpha_{11}^{cn}}{4\alpha'_{111}P_0^2 + \alpha_{11}^{cn}}. \tag{51}$$

The width of such a strictly charge-neutral head-to-tail domain wall reads

$$2\xi_{HT2} = 2\xi'\sqrt{A} = \frac{2}{P_0}\sqrt{\frac{G'_{66}}{6\alpha'_{111}P_0^2 + \alpha_{11}^{cn}}} = P_0\sqrt{\frac{G'_{66}}{f_{HT2} - f_{EL0}}}, \tag{52}$$

where the Euler-Lagrange potential at the domain-wall center is now approximated by

TABLE III. Thickness of domain walls in $BaTiO_3$ at ambient conditions, calculated from the present model according to the definition (43). Here $2\xi_{HH1}$ and $2\xi_{HT1}$ stand for fully relaxed head-to-head and head-to-tail domain walls in the model without the depolarization energy, $2\xi_{HT}$ stands for the fully relaxed head-to-tail domain wall in the complete model, $2\xi_{HT2}$ stands for value calculated using approximation (52), and $2\xi_{180}$ stands for the thickness of the 180° domain wall evaluated from Eq. (59).

	I	II	III	Unit
$2\xi_{HH1}$	8.64	8.62	8.41	nm
$2\xi_{HT1}$	9.36	9.40	9.24	nm
$2\xi_{HT2}$	3.59	3.57		nm
$2\xi_{HT}$	3.59	3.58	3.69	nm
$2\xi_{180}$	0.63	0.65	0.67	nm

$$f_{HT2} = \frac{1}{2}\alpha_1^s P_0^2 + \frac{1}{4}\alpha_{11}^s P_0^4 + \frac{1}{8}\alpha'_{111} P_0^6. \tag{53}$$

The numerical values of $2\xi_{HT2}$ for room-temperature $BaTiO_3$ are given in Table III. It is obvious that the $2\xi_{HT2}$ estimate is really very close to the domain-wall width of the exact solution

$$2\xi_{HT} = P_0 \sqrt{\frac{G'_{66}}{f_{HT} - f_{EL0}}}, \tag{54}$$

where f_{HT} is the true saddle-point value of $f_{EL}+f_{EL2}$, given by the minimum value of the potential

$$f_{EL2}(P_s,0) = \alpha_1^s P_s^2 + \alpha_{11}^s P_s^4 + \alpha'_{111} P_s^6 + \frac{1}{2\epsilon_B \epsilon_0}(P_s - P_0/\sqrt{2})^2. \tag{55}$$

Once the domain-wall profile [course of $P_s(s), P_r(s), e_\alpha(s)$] is known, the domain-wall energy Σ_{90} can be calculated from the path integral

$$\Sigma_{90} = \int_{-\infty}^{\infty} \{f_{EL2}[P_s(s), P_r(s)] - f_{EL0}\} ds = 2\int_{-\infty}^{\infty} f_G \, ds. \tag{56}$$

In the strict charge-neutral approximation (div $\mathbf{P}=0$), the head-to-tail domain-wall energy reads

$$\Sigma_{HT2} = \frac{G'_{66} P_0^2}{2\xi'} A^2 I(A), \tag{57}$$

where ξ' and A are given by Eq. (51) and $I(A)$ is a numerical factor[67]

$$I(A) = \int_{-\infty}^{\infty} \frac{\cosh(t)^2 \, dt}{[A + \cosh(t)^2 - 1]^3}, \tag{58}$$

depending on the deviation of the domain-wall profile from the $\tanh(s)$ shape.

TABLE IV. Experimental estimates of 90° wall thickness in $BaTiO_3$. TEM, AFM, and SNOM stand for transmission electron microscopy, atomic force microscopy, scanning near-field optical microscopy.

Model	90° wall thickness [nm]	Source (Year)
TEM	20	Ref. 64 (1964)
TEM	4–6	Ref. 33 (1972)
TEM	7–12	Ref. 30 (1974)
Electron holography	1–2.5	Ref. 26 (1992)
Electron holography	2–5	Ref. 27 (1993)
X-ray diffraction	4–6	Ref. 28 (1997)
X-ray diffraction	14	Ref. 29 (1999)
AFM/SNOM	25	Ref. 32 (2000)

V. DISCUSSION

A. Domain-wall thickness

We note that the thickness of a fully relaxed 90° domain wall in our models is about one order of magnitude larger than the unit cell size, so that the resulting microscopical displacement profile is really smooth. The predicted value itself (about 3.6–3.7 nm) is in reasonable agreement with various experimental estimates, resumed in Table IV. When judging the experimental values, one has to bear in mind that there is no straightforward way of measuring the spatial profile of polarization across the domain wall so that the provided experimental values should rather be considered as apparent widths that tend to overestimate the actual thickness. Other reasons for the overestimation could be effects of lateral resolution, residual strain, roughening by thermal fluctuations or defects,[65] possible broadening due to proximity of the crystal surface,[66] and so on. Moreover, the present calculation suggests that if the depolarization charge can be screened out by mobile charges, the domain wall would actually approach $2\xi_{HT1}$ (about 9 nm). The only method that predicts very sharp domain walls is electron holography.[26,27] The value in the earlier paper[26] is even lower than our prediction but such an underestimation may possibly come from the approximations employed in the evaluation[26,27] of the domain-wall thickness from the observed electron interferograms.

The frequently cited theoretical estimate of 90° twin boundaries given in Ref. 31 is that calculated by Zhirnov[17] ($2\xi_{HT2}=10-20$ nm). This calculation is surprisingly good taking into account that it was based on a fourth-order Landau potential and a rather crude estimation of model parameters. A similar rough estimate (giving 2 nm) was given in Ref. 67 which employs a sixth-order Landau potential but the domain wall is not a fully relaxed (strain was evaluated from $e_\alpha=0$ rather than from $\partial e_\alpha/\partial s=0$) condition. We are not aware of any more advanced calculations of 90° twin boundaries in $BaTiO_3$.

In this paper, we have not investigated properties of 180° domain walls. The case of the basic planar uncharged 180° wall is, however, quite simple: the depolarization term can be

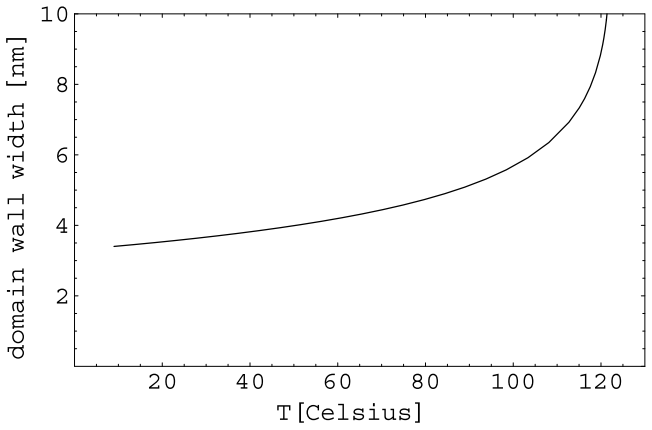

FIG. 6. Thickness of a 90° domain wall as a function of temperature, calculated for model I with Landau potential parameters varying according to the Ref. 44.

dropped out and there is only a single Euler-Lagrange equation. The problem was treated, e.g., in Ref. 21. The expression for its thickness can be obtained in the form

$$2\xi_{180} = 2P_0\sqrt{\frac{G_{44}}{2E_B}}, \tag{59}$$

where the barrier on the associated Euler-Lagrange potential is in case of the sixth-order Landau expansion simply:

$$E_B = \left(\alpha_{11}^{(e)} - \frac{q_{12}^2}{2C_{11}}\right)P_0^4 + 2\alpha_{111}P_0^6. \tag{60}$$

The domain-wall energy can be expressed as

$$\Sigma_{180} = \frac{G_{44}P_0^2}{\xi_{180}}A_{180}^4 I(A_{180}), \tag{61}$$

where

$$A_{180} = \frac{3\alpha_{111}P_0^2 + \alpha_{11}^{(e)} - \frac{q_{12}^2}{2C_{11}}}{2\alpha_{111}P_0^2 + \alpha_{11}^{(e)} - \frac{q_{12}^2}{2C_{11}}} \tag{62}$$

and $I(A)$ is given by Eq. (51). The expression (59) gives thickness of about 0.63 nm (0.65 nm, 0.67 nm) for model I (models II, III) and a domain-wall energy of about 6 mJ/m^2. Such values are in nice agreement with the independent *ab initio* calculations of Ref. 76 (0.56 nm, 7–16 mJ/m^2). Let us stress that even here, the domain thickness is larger than the unit cell (0.4 nm).

B. Temperature evolution

The domain-wall thickness and profile can considerably change with temperature or pressure. The properties of the 90° domain wall of $BaTiO_3$ can be calculated in our model in at any temperature within stability limits of the tetragonal phase. The temperature dependence of the Landau potential coefficients as given in Refs. 41 and 44 gives the temperature evolution of the domain-wall thickness as shown in Fig. 6. An increase of the domain-wall thickness with temperature is the usual trend and it was also seen[30] in experiments.

It should be stressed that in the room-temperature case discussed earlier, the head-to-head and head-to-tail central states correspond to the true saddle points of the potential f_{EL}. In general, however, the domain-wall center may become a local minimum. Our derivations are also valid in this case except that the domain center is no longer the point with the largest gradient of the polarization. This is expected to happen in the vicinity of the tetragonal-orthorhombic phase transition. For f_{EL} of model I it happens already at 24 °C. Nevertheless, the influence of the coexisting local minimum on the domain wall profile is quite small here and it is anyway removed when the dipole-dipole interaction term is included.

C. Symmetry considerations

The 90 domain wall profiles considered here are described by a polarization field which has a normal component P_s and a tangential component P_r. As mentioned earlier, these components are for head-to-tail domain-wall even and odd functions of s, respectively $[P_s(s)=P_s(-s)$ and $P_r(s)=-P_r(-s)]$. Therefore, the associated polarization field P is symmetric in the sense that there is this unique relation between the shape of the wall on the opposite sides from the central plane $s=0$, which can be identified with the domain-wall center.

The realistic atomic structure of such a domain wall can be in principle derived from the reference cubic structure by applying atomic shifts similar to that of the soft mode,[68] with vectorial amplitudes proportional to the superposed polarization field with components $(P_s(s), P_r(s))$. Irrespectively of the central plane position, the layer symmetry[69] of the resulting atomic arrangement[68] would be m_z. As such atomic structure does not have a symmetry element relating points at opposite sides of the central plane, it should be considered as asymmetric, in agreement with the rigorous symmetry analysis of Ref. 69). Clearly, the asymmetry of the domain wall itself (as defined in Ref. 69) does not exclude possibility to describe it as a reference atomic structure with displacements modulated by odd and even functions of s.

It was also argued that the asymmetry of the head-to-tail domain wall allows for a residual charge distribution in the form of a dipole layer.[70] On passing through the domain wall, this dipole layer creates a step in the macroscopic electrostatic potential. The unscreened magnitude of this step,[70]

$$\Delta\phi = -\frac{1}{\epsilon_0}\int [P_r(s) - P_0/\sqrt{2}]ds, \tag{63}$$

in the fully relaxed head-to-tail wall in model I is about 0.5 eV, which is quite comparable with the first-principles-based estimate[70] for $PbTiO_3$ (0.18 eV). Finally, according to definitions of Ref. 71, these head-to-tail solutions are chiral.

D. Model parameters

In this work, we have determined gradient coefficients from an inelastic neutron scattering experiment. We estimate that the error in the determination of G_{11} and G_{44} is about 5%

and 25%, respectively. These uncertainties are probably the principal limiting factor in predictions of the 90° and 180° domain wall widths. At the same time, the available data are insufficient for a quantitative estimate of G_{12}. This does not really matter here, since G_{12} appears in the calculations always together with the much larger coefficient G_{11}, but it should be kept in mind when applying the present model parameters to other problems. In fact, we are not aware of any previous determination of the gradient tensor in $BaTiO_3$. For example, the predictions of Ref. 17 are based on a very rough guess that $G_{11} \approx \alpha_1(0)d^2$, where $\alpha_1(0)$ is a low temperature value α_1 and d is a lattice constant; Refs. 36 and 37 adopt another estimate giving $G_{11}=250\times10^{-11}$ J m^3 C^{-2} while Ref. 8 has simply chosen $G_{11}=1.38\times10^{-11}$ J m^3 C^{-2} in order to receive sharper domain walls, and others have just worked with rescaled, dimensionless variables.[34,35,38] None of these previous works has considered the huge anisotropy $G_{11} \gg G_{44}$, which is essential for reproducing the relative size and energy 90° and 180° domain walls, as apparent from Eqs. (54), (57), (61), and (59). In any case, additional experiments or first-principles calculations could be helpful for the determination of all these gradient coefficients with more precision.

In addition to this, there is a legitimate concern that all Landau coefficients do depend on temperature[72–75] and, moreover, on the order of the Landau potential expansion.[72,73] By the way, the latter is apparent from Table I, too. There are also valid arguments[75] against the model with sixth-order expansion only. Such a discussion, however, is not in conflict with the present work. Both sixth- and eighth-order potentials considered here were constructed in a way to reproduce reasonably quantities like susceptibility, transition entropies, spontaneous polarization, energy differences between the tetragonal and orthorhombic states, and so on. Here it is merely this kind of (reliable) basic quantities through which the (somewhat ambiguously defined) coefficients appear in present calculations. For example, inspection of Eq. (54) suggests that the head-to-tail domain wall width depends primarily on the energy difference between the single-domain state and the intermediate orthorhombic state inside the wall, the spontaneous polarization, and the gradient coefficients. Therefore, we do not expect much error here in choosing a sixth-order model instead of an eighth-order model, although the eighth-order model may be in principle better adjusted. One should keep in mind, however, that for quantitative calculations of other phenomena, like those[75] which rely on the nonlinear response to high electric fields, the present model may turn out to be insufficient.

VI. CONCLUSION

In this work, we have completed the available Devonshire model of $BaTiO_3$ by quantitative appreciation of the dipole-dipole and the highly anisotropic gradient interactions. Within this model, the basic properties of 90° domain walls were analyzed in detail. It was found that flat (charged) head-to-head 90° domain walls are not stable at ambient conditions. The thickness $2\xi_{HT}$ of the head-to tail 90° wall and thickness $2\xi_{180}$ of the 180° wall were calculated as a function of temperature and found to be in acceptable agreement with available experimental data and a first-principles-based model.[76] As ξ_{HT} and ξ_{180} play the role of polarization-polarization correlation lengths in the ferroelectric phase, we believe that the same set of parameters values should allow realistic calculations of other $BaTiO_3$ domain-wall phenomena or problems with inhomogeneous order parameters.

The success of the quantitative predictions for $BaTiO_3$ indicates that the earlier proposed[24,51] program—to derive all parameters in the model from bulk properties—is feasible and useful for ferroelectric perovskites in general. Application of the program to other materials is beyond the scope of this work but it is worth noting that all the calculations given here apply directly to tetragonal phases of ferroelectric perovskites like $PbTiO_3$ or $KNbO_3$. Clearly, numerous analytical expressions derived here [e.g., the expression for thickness and energy of the strictly charge-neutral head-to-tail domain wall given in Eqs. (52), (53), (57), and (58) or the formulas for 180° wall given in Eqs. (59)–(62)] can be thus useful in analyzing of such materials, too. Whether the parameters come from the experiment or first-principles studies, the model given by Eqs. (1)–(6) gives the possibility of quantitative simulations of domain-wall or inhomogeneous polarization phenomena at scales of the order of 1–100 nm in a variety of interesting insulating ferroelectrics.

ACKNOWLEDGMENTS

This work has been supported by the Grant Agency of the Czech Republic (Projects Nos. 202/05/H003 and 202/06/0411).

[1] X. B. Ren, Nat. Mater. **3**, 91 (2004).
[2] S. E. Park, S. Wada, L. E. Cross, and T. R. Shrout, J. Appl. Phys. **86**, 2746 (1999).
[3] S. Wada, S. Suzuki, T. Noma, T. Suzuki, M. Osada, M. Kakihana, S. E. Park, L. E. Cross, and T. R. Shrout, Jpn. J. Appl. Phys., Part 1 **38**, 5505 (1999).
[4] S. Wada and T. Tsurumi, Br. Ceram. Trans. **103**, 93 (2004).
[5] K. Yako, H. Kakemoto, T. Tsurumi and S. Wada, Mater. Sci. Eng., B **120**, 181 (2005).
[6] S. Wada, K. Yako, H. Kakemoto, T. Tsurumi, and T. Kiguchi, J. Appl. Phys. **98**, 014109 (2005).
[7] J. J. Liu, Y. C. Zhou, A. K. Soh, and J. Y. Li, Appl. Phys. Lett. **88**, 032904 (2006).
[8] R. Ahluwalia, T. Lookman, A. Saxena, and W. Cao, Phys. Rev. B **72**, 014112 (2005).
[9] J. Fousek and V. Janovec, J. Appl. Phys. **40**, 135 (1969).
[10] J. Sapriel, Phys. Rev. B **12**, 5128 (1975).
[11] E. Little, Phys. Rev. **98**, 978 (1955).
[12] J. Han and W. Cao, Appl. Phys. Lett. **83**, 2040 (2003).
[13] J. Han and W. Cao, J. Appl. Phys. **87**, 7438 (2000).

[14] X. Tan and J. K. Shang, J. Appl. Phys. **95**, 635 (2004).
[15] X. Tan and J. K. Shang, J. Appl. Phys. **96**, 2805 (2004).
[16] C. A. Randall, D. J. Barber, and R. W. Whatmore, J. Mater. Sci. **22**, 925 (1987).
[17] V. A. Zhirnov, Zh. Eksp. Teor. Fiz. **35**, 1175 (1958) , [Sov. Phys. JETP **35**, 822 (1959)].
[18] Y. Ishibashi and E. Salje, J. Phys. Soc. Jpn. **71**, 2800 (2002).
[19] Y. Ishibashi, J. Phys. Soc. Jpn. **62**, 1044 (1993).
[20] Y. Ishibashi and V. Dvorak, J. Phys. Soc. Jpn. **41**, 1650 (1976).
[21] W. Cao and L. E. Cross, Phys. Rev. B **44**, 5 (1991).
[22] V. Dvorak and V. Janovec, Jpn. J. Appl. Phys. **4**, 400 (1965).
[23] I. Rychetsky and W. Schranz, J. Phys.: Condens. Matter **5**, 1455 (1993).
[24] W. Cao and G. R. Barsch, Phys. Rev. B **41**, 4334 (1990).
[25] W. Cao, G. R. Barsch, and J. A. Krumhansl, Phys. Rev. B **42**, 6396 (1990).
[26] X. Zhang, T. Hashimoto, and D. C. Joy, Appl. Phys. Lett. **60**, 784 (1992).
[27] X. Zhang, D. C. Joy, Y. Zhang, T. Hashimoto, L. Allard, and T. A. Nolan, Ultramicroscopy **51**, 21 (1993).
[28] N. Floquet, C. M. Valot, M. T. Mesnier, J. C. Niepce, L. Normand, A. Thorel, and R. Kilaas, J. Phys. III **7**, 1105 (1997).
[29] N. Floquet and C. Valot, Ferroelectrics **234**, 107 (1999).
[30] M. D. Dennis and R. C. Bradt, J. Appl. Phys. **45**, 1931 (1974).
[31] M. E. Lines and A. M. Glass, *Principles and Applications of Ferroelectrics and Related Materials* (Clarendon, Oxford, 1979).
[32] L. M. Eng and H. J. Guntherodt, Ferroelectrics **236** 35 (2000).
[33] S. I. Yakunin, V. V. Shakmanov, G. V. Spivak, and N. V. Vasil'eva, Fiz. Tverd. Tela (S.-Peterburg) **14**, 373 (1972) [Sov. Phys. Solid State **14**, 310 (1972)].
[34] H. L. Hu and L. Q. Chen, Mater. Sci. Eng., A **238**, 182 (1997).
[35] H. L. Hu and L. Q. Chen, J. Am. Ceram. Soc. **81**, 492 (1998).
[36] R. Ahluwalia, T. Lookman, A. Saxena, and W. Cao, Appl. Phys. Lett. **84**, 3450 (2004).
[37] R. Ahluwalia, T. Lookman, A. Saxena, and W. Cao, cond-mat/0308232 (unpublished).
[38] S. Nambu and D. A. Sagala Phys. Rev. B **50**, 5838 (1994).
[39] A. F. Devonshire, Philos. Mag. **40**, 1040 (1940).
[40] J. F. Nye, *Physical Properties of Crystals* (Oxford University Press, Oxford, 1985).
[41] A. J. Bell, J. Appl. Phys. **89**, 3907 (2001).
[42] The difference between the α_{11}^0 and α_{11} coefficients (defining "clamped" and "relaxed" potentials) correspond to the difference between α_{11}' and α_{11} in Ref. 38 and between ξ_{11}'' and ξ_{11}' in Ref. 39, respectively.
[43] Y. F. Gao and Z. Suo, J. Appl. Mech. **69**, 419 (2002).
[44] A. J. Bell and L. E. Cross, Ferroelectrics **59**, 197 (1984).
[45] Y. L. Li, L. E. Cross, and L. Q. Chen, J. Appl. Phys. **98**, 064101 (2005).
[46] Z. Li, S. K. Chan, M. H. Grimsditch, and E. S. Zouboulis, J. Appl. Phys. **70**, 7327 (1991).
[47] D. Berlincourt and H. Jaffe, Phys. Rev. **111**, 143 (1958).
[48] M. Zgonik, P. Bernasconi, M. Duelli, R. Schlesser, P. Gunter, M.H. Garrett, D. Rytz, Y. Zhu, and X. Wu, Phys. Rev. B **50**, 5941 (1994).
[49] S. Ding *et al.*, Chin. Phys. Lett. **22**, 1790 (2005).
[50] T. Yamada, J. Appl. Phys. **43**, 328 (1972).
[51] W. Cao, J. Phys. Soc. Jpn. **63**, 1156 (1994).
[52] J. Hlinka, J. Petzelt, S. Kamba, D. Noujni, and T. Ostapchuk, Phase Transitions **79**, 163 (2006).
[53] J. Harada, J. D. Axe, and G. Shirane, Phys. Rev. B **4**, 155 (1971).
[54] Ph. Ghosez, E. Cockayne, U. V. Waghmare, and K. M. Rabe, Phys. Rev. B **60**, 836 (1999).
[55] Y. Yamada, G. Shirane, and A. Linz, Phys. Rev. **177**, 848 (1969).
[56] J. Hlinka and E. Klotins, J. Phys.: Condens. Matter **15**, 5755 (2003).
[57] A. K. Tagantsev, E. Courtens, and L. Arzel, Phys. Rev. B **64**, 224107 (2001).
[58] J. L. Servoin, F. Gervais, A. M. Quittet, and Y. Luspin, Phys. Rev. B **21**, 2038 (1980).
[59] J. Wang, S. Q. Shi, L. Q. Chen, Y. Li, and T. Y. Zhang, Acta Mater. **52**, 749 (2004).
[60] J. Wang, Y. Li, L. Q. Chen, and T. Y. Zhang, Acta Mater. **53**, 2495 (2005).
[61] S. A. Hayward and E. K. H. Salje, J. Phys.: Condens. Matter **14**, L599 (2002).
[62] V. B. Shirokov, V. I. Torgashev, A. A. Bakirov, and V. V. Lemanov, Phys. Rev. B **73**, 104116 (2006).
[63] N. A. Pertsev, A. G. Zembilgotov, and A. K. Tagantsev, Phys. Rev. Lett. **80**, 1988 (1998).
[64] M. Tanaka and G. Honjo, J. Phys. Soc. Jpn. **19**, 954 (1964).
[65] B. M. Darinskii and A. S. Sidorkin, Fiz. Tverd. Tela (Leningrad) **26**, 3410 (1984).
[66] B. M. Darinskii, A. P. Lazarev, and A. S. Sidorkin, Fiz. Tverd. Tela (Leningrad) **31**, 287 (1989).
[67] L. N. Bulaevskii, Fiz. Tverd. Tela (Leningrad) **5**, 3183 (1963).
[68] V. Janovec, M. Grocky, V. Kopsky, and Z. Kluiber, Ferroelectrics **303**, 65 (2004).
[69] V. Janovec and J. Privratska, in *International Tables for Crystallography* (Kluwer Academic, Dordrecht, 2003), Chap. 3.4, Vol. D.
[70] B. Meyer and D. Vanderbilt, Phys. Rev. B **65**, 104111 (2002).
[71] B. Houchmandzadeh, J. Lajzerowicz, and E. Salje, J. Phys.: Condens. Matter **3**, 5163 (1991).
[72] A. Troster, C. Dellago, and W. Schranz, Phys. Rev. B **72**, 094103 (2005).
[73] S. Radescu, I. Etxebarria, and J. M. Perez-Mato, J. Phys.: Condens. Matter **7**, 585 (1995).
[74] V. V. Shvartsman and A. L. Kholkin, Phys. Rev. B **69**, 014102 (2004).
[75] Y. L. Wang, A. K. Tagantsev, D. Damjanovic, N. Setter, V. K. Yarmarkin, and A. I. Sokolov, Phys. Rev. B **73**, 132103 (2006).
[76] J. Padilla, W. Zhong, and D. Vanderbilt, Phys. Rev. B **53**, R5969 (1996).